

Wind Turbine Blades as a Strain Energy Source for Energy Harvesting

Dong-Won Lim, Susan C. Mantell, Peter J. Seiler, Rusen Yang
University of Minnesota, Minneapolis, MN, 55455

Structural health monitoring of wind turbine blade mechanical performance can inform maintenance decisions, lead to reduced down time and improve the reliability of wind turbines. Wireless, self-powered strain gages and accelerometers have been proposed to transmit blade data to a monitoring system located in the nacelle. Each sensor node is powered by a strain Energy Harvester (EH). The amplitude and frequency of strain at the blade surface (where the EH is mounted) must be sufficient to enable data transfer. In this study, the strain energy available for energy harvesting is evaluated for three typical wind turbines with different wind conditions. A FAST simulation code, available through the National Renewable Energy Lab (NREL), is used to determine bending moments in the wind turbine blade. Given the moment data as a function of position along the blade and time (i.e. blade rotational position), strain in the blade is calculated. The data provide guidance for optimal design of the energy harvester.

Nomenclature

E	=	Modulus of an EH [GPa] ($E_0 = 1$ GPa)
$EI_{E(F),i}$	=	Stiffness in edge(flap)-wise bending at i th element [Nm^2]
K_{EH}	=	Design factor [m^3]
$M_{E(F),i}$	=	Edge(Flap)-wise moment at i th node [Nm]
P_{avail}	=	Strain power available [μW]
V	=	Volume of an EH [m^3]
W_{strain}	=	Harvested strain energy [μJ]
c_i	=	Chord length of i th airfoil [m]
f	=	Strain frequency [Hz]
t_i	=	Thickness of i th airfoil [m]
Δt	=	Charging time [sec]
ε	=	Mechanical strain [$\mu\text{-}\varepsilon$]
η	=	Energy conversion efficiency[-]

I. Introduction

THE DOE has set a goal of “20% wind energy by 2030”.¹ Reduction in operating and maintenance costs for wind turbines has been identified as a major challenge to achieving this goal. Wind turbine maintenance is a particular challenge because wind turbines are often located in remote regions (including offshore). Structural health monitoring (SHM) is a promising approach that can enable preventative maintenance, reduce down time and significantly reduce life-cycle costs.² While failure can occur in any structural component, one of the most common and critical components to fail is

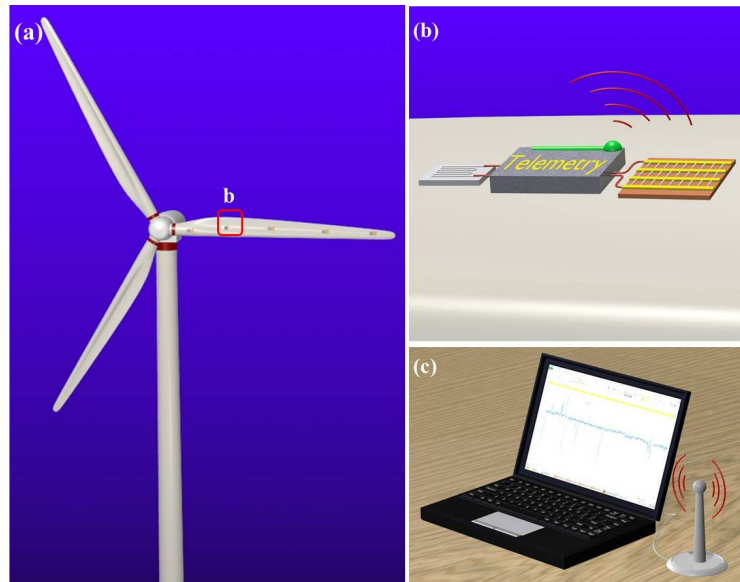


Figure 1. Schematic showing (a) sensor nodes mounted on blade, (b) node with energy harvester and telemetry, and (c) data acquisition and health monitoring.

the wind turbine blade.³ It is particularly challenging to continuously monitor blade health: (1) the blades are quite long and an extensive network of sensors is required; and (2) the blades are rotating, posing challenges to delivering power to and receiving data from the sensor network. To address these issues, a novel sensing and SHM system has been proposed (Figure 1). The system is comprised of a network of sensor nodes (Figure 1(a)). Each node is powered by an energy harvester (EH) and includes a sensor and telemetry unit (Figure 1(b)). The strain gauge and/or accelerometer data will be wirelessly transmitted to a centralized monitoring system in the turbine nacelle (Figure 1(c)). Recent technological developments in energy harvesting materials and fabrication processes along with commercially available low power telemetry modules make these technology advancements a possibility for the first time.

In the present study, the availability of strain energy for various commercially available wind turbines will be evaluated.

II. Background

A. Sensors and Telemetry for Structural Health Monitoring

Damage to the composite blade often begins as a matrix crack that can lead to debonding and delamination as the blade undergoes cyclic loading. A variety of sensing approaches have been considered for structural health monitoring of composite structures such as helicopter or wind turbine blades including: acoustic sensors, accelerometers, strain gauges, piezoceramic transducers and fiber optic sensors.⁴⁻⁸ These sensors typically provide strain, acceleration and acoustic/vibration data in real time. Sensor data is processed using algorithms designed to predict the location and extent of damage based on sensor data. Ciang et al.⁹ completed an extensive review of sensors for damage detection and their suitability as an SHM system for wind turbine blades. Sensors that provide acoustic emission, thermal imaging, and ultrasound data can provide overall health but are difficult to interpret because the blade geometry is complex. These authors identified “hot spots” on the blade where failure is likely to occur. These hot spots include the blade root, 30% span from the root, and 70% span from the root. Even so, damage detection requires *multiple* sensors “in the vicinity” of the anticipated damage location. Discrete sensors such as strain gauges and accelerometers are acceptable as long as there are clusters of these sensors located near anticipated damage sites to ensure proximity to (and detection of) damage. With many sensors, the challenge becomes powering the sensors and relaying the data to a central data acquisition system for further processing.

B. Feasibility of Energy Harvesting

In the present study, the feasibility of an EH for wind turbine blade SHM has been investigated. One aspect of this study has been to verify that the strain energy available during typical operating conditions can satisfy the power requirements for sensing and telemetry. A data acquisition and power management strategy is considered such that “harvested” energy is stored in a capacitor until a threshold energy level is achieved. Once the stored energy is sufficient for data acquisition and telemetry, strain data for several complete revolutions of the wind turbine are wirelessly transferred to a data acquisition substation as a burst. At which point, the energy harvester restores the capacitor and the data cycle begins again. Feasibility, then, entails estimating the power requirements and the power available to be harvested.

The strain energy harvested W_{strain} will depend on the energy harvester configuration, the frequency f and sinusoidal amplitude of the strain ε :

$$W_{\text{strain}} = \eta VE \cdot \varepsilon^2 f \cdot \Delta t \quad (1)$$

where V is the volume of an EH, E is the modulus of the EH, and η is the efficiency of energy conversion. The charging time Δt is the time required to charge the capacitor and will also define the time between bursts of data transmission/acquisition. The magnitude of strain and frequency will depend on the wind turbine blade geometry and operating conditions. For example, it has been reported that flapwise and edgewise bending of the blade can provide strain ranging from 1200 $\mu\varepsilon$ (1.65 MW turbine)¹² to 3600 $\mu\varepsilon$,^{13,14} at 0.25 Hz.

As noted, the energy available for harvesting depends on the strain and the frequency of vibration; and harvesting capability depends on the type and the design of an EH (Eq. (1)). Thus is useful to define the power available P_{avail} and the EH design factor K_{EH} as

$$P_{\text{avail}} = E_0 \varepsilon^2 f \quad (2)$$

$$K_{EH} = \eta V \frac{E}{E_0} \quad (3)$$

where E_0 is the nominal modulus of an EH material. By using this measure of power, simulation strain data can be compared for various turbines and under various operating conditions. For the purpose of comparison, a modulus of $E_0 = 1$ GPa is taken in all plots and data reported herein. Values can easily be scaled to evaluate other harvester materials. So, the harvested energy can be decomposed into an internal factor (K_{EH}) and external source (P_{avail} and Δt). Now, one can determine the type and size of an EH from K_{EH} with selected charging time. And the original Eq. (1) is simplified into

$$W_{strain} = P_{avail} \cdot K_{EH} \cdot \Delta t. \quad (4)$$

While these studies provide a good starting point for estimating the strain energy available, a map of strain over the blade surface will be required to accurately assess the energy harvester design. The objective of this study is to characterize the strain energy available for a range of wind turbines under steady state and turbulent conditions. Three turbines have been selected that represent typical turbine power capacities and geometries: a CART3 (600 kW), a WindPact (1.5 MW) and a 5MW offshore wind turbine. Wind loading conditions are varied from 6 to 24 m/s at high and low turbulence.

III. Methods

There are a number of options available for creating a detailed finite element model of wind turbine blades. For example, NuMAD¹⁵ is a pre and post processor (for use with ANSYS) with a graphical user interface that enables users to quickly create a three dimensional model of a wind turbine blade. One drawback to these models is that extensive knowledge of the blade geometry and composite material layup is required. This detailed information is considered proprietary by commercial wind turbine manufacturers. Instead, nonlinear simulations presented in this paper are performed using the FAST (Fatigue, Aerodynamics, Structures, and Turbulence) aeroelastic design code for horizontal axis wind turbines developed by the National Renewable Energy Laboratory (NREL)¹⁶. In FAST the wind turbine is modeled as an interconnected system of rigid bodies (i.e., the nacelle and hub) and flexible bodies (i.e., the blades, tower and drive shaft) subjected to dynamic wind loads. FAST uses the assumed modes method for the flexible structural dynamics of the system and blade element momentum theory is used to calculate the aerodynamic loads using AeroDYN.¹⁷ FAST can model wind turbines with a total of 22-24 degrees of freedom. This full order model includes first and second tower fore-aft and side-to-side bending modes, first and second flapwise bending modes of blades, first edgewise bending modes of blades, drive train torsion, generator position and nacelle yaw angle. Input data to the FAST code includes the turbine geometry and component material properties along with wind loading and aerodynamic data. Standard output data include blade displacement, such as flap-wise and edge-wise displacement, forces and bending moments as a function of rotation.

A number of predefined, FAST turbine models have been constructed and are available through the NREL FAST website. These models can be used to characterize the available strain energy for turbines of various sizes. Specifically, this paper will focus on three different turbine models: a) 1.5 MW WindPact, b) 600kW CART3, and c) 5MW off-shore. The specifications of each turbine are shown in **Table 1**. In each simulation the standard, built-in control law is used to generate the generator torque and blade pitch commands.

Table 1. Three Typical Wind Turbines Properties

Index	CART3	WindPACT	NREL Offshore
Rated Power	600 kW	1.5 MW	5.0 MW
Rated Rotor Speed	37.1 rpm	20.5 rpm	12.1 rpm
Cut-in, Rated, Cut-out Wind Sp	6, 13.5, 20 m/s	3, 11.5, 27.6 m/s	3, 11.4, 25 m/s
Hub Height	34.86 m	84 m	87.6 m
Blade Length (Radius)	20 m	35 m	63 m
Blade Weight	1,807 kg	3,913 kg	17,740 kg
Blade Airfoil Type	s816, 817, 818	s818, 825, 826	DU21, 25, 30, 35, 40
References	Ref. 18	Ref. 19	Ref. 20

Blade strain is not calculated as part of the standard outputs from FAST. However, the FAST outputs include moments and deflections at various locations (nodes) along the span of the blades. These can be used to calculate strains in several ways: 1) local span (nodal) moments, 2) local span translational deflections, 3) blade tip deflection with a mode-shape function, and 4) blade root moments with a mode-shape. Strains calculated using mode-shapes are not accurate because the mode-shapes are only approximately correct and may not correspond to the actual blade

mode in operation. On the other hand, nodal moment outputs can be used to compute accurate local strains at various nodal locations. Hooke's law provides the following relationship between strain ε and moment M :

$$\varepsilon_e(z_b) = \frac{\sigma}{E} = \frac{M_e(z_b)y_b}{EI}, \text{ and } \varepsilon_f(z_b) = \frac{\sigma}{E} = \frac{M_f(z_b)x_b}{EI} \quad (5)$$

where ε denotes the strain, M is the bending moment, EI is stiffness, z_b is the distance from the blade support at the nacelle to the node, and x_b/y_b are the chord length and thickness of the airfoil. Eq. (5) assumes pure bending mode is the dominant factor. The subscripts e and f denote the edge and flapwise directions on the blade. **Figure 2** (left) shows the coordinate system of blades. Each bending direction is depicted in **Figure 2** (right). Bending strain (or stress) is proportional to the distance from the neutral axis crossing the mass center. Therefore, x_b is the direction of the distance for the edgewise strain and y_b is for the flapwise strain.

These strains are greatest at the maximum distance as shown in **Figure 2** (right). For the maximum edgewise strain, the chord length $y_b=c/2$ of the airfoil is used and the thickness $x_b=t/2$ yields the maximum flapwise strain. The airfoil geometry of a wind turbine blade is generally quite complicated and finding the neutral axis is nontrivial. A reasonable approximation is to use half the local thickness and chords length to estimate the maximum edge and flapwise strain. The FAST simulation allows up to nine nodal moment outputs. These can be used to compute strain at the nine discrete locations along the span of the blade. Specifically, at the i^{th} local nodes, the edgewise and flapwise strain can be expressed as in Eq. (6)

$$\varepsilon_{e,i} = \frac{M_{E,i}c_i}{2(EI)_{E,i}}, \text{ and } \varepsilon_{f,i} = \frac{M_{F,i}t_i}{2(EI)_{F,i}} \quad (6)$$

where c_i and t_i are the chord length and thickness of the airfoil at the i^{th} node.

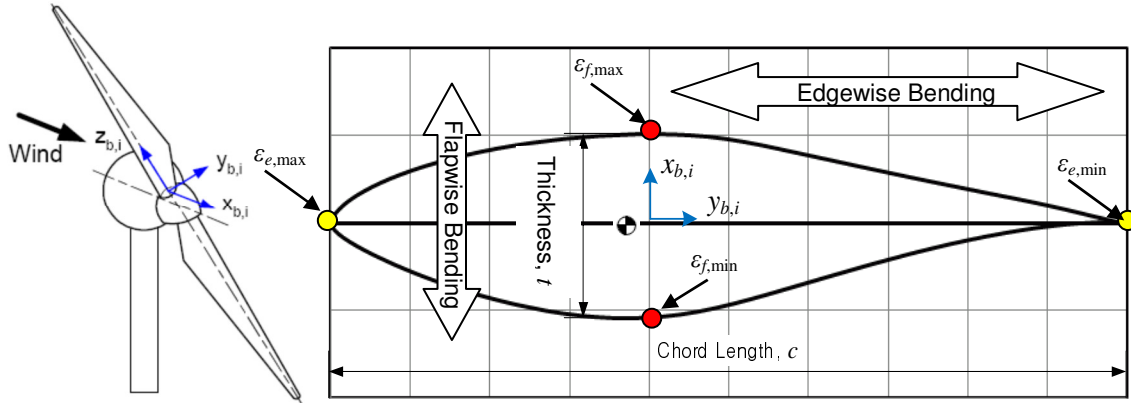


Figure 2. Blade Coordinate System (left)¹⁶ and Cross-sectional Shape of Blade (right): Max. Strain Locations

IV. Results and Discussion

Simulations were performed for turbines of three sizes and at different wind speed and turbulence conditions. Simulation results for the 5MW NREL offshore wind turbine operating under wind conditions of 24 m/s at low turbulence are shown in **Figure 3** and **Figure 4**. **Figure 3** shows strain data in both edgewise and flapwise bending at an instant in time and Fast Fourier Transform analysis of each bending mode. **Figure 4** shows the edgewise and flapwise strain power along the span of the blade during the operation under the selected wind conditions. As shown in **Figure 3**, the amplitude of the edgewise strain is ~ 550 micro-strain and the amplitude of the flapwise strain is ~ 390 micro-strain. The strain varies with time at a cyclic rate of ~ 0.34 Hz, corresponding to the rotational frequency of the turbine at these wind conditions. For the flapwise bending mode, large non-zero mean strain is observed. But this bias term is disregarded, as the zero-frequency mode does not contribute to generate energy. In **Figure 4**, the maximum edgewise strain power, $\sim 60 \text{ W/m}^3$, occurs at a distance 15.9 m from the blade support (at the nacelle). On the contrary, the maximum flapwise strain power, $\sim 31 \text{ W/m}^3$, occurs at 40.5 m. A similar flapwise strain power of 30 W/m^3 occurs at 15.9 m.

Similar simulations were performed for the CART3 and WindPACT turbine models to assess the available energy for harvesting. **Table 2** summarizes the results of these simulations. The maximum strain, strain frequency and spanwise location of the maximum strain are shown for both edgewise and flapwise bending. Several trends are

apparent in these results. First, the strain progressively increases with increasing turbine size. This is expected as the 5MW turbine has larger, more flexible blade leading to increasing strain. Second, the strain is greatest at the higher wind speed/lower turbulence intensity conditions. Third, the frequency of maximum strain tends to match with the rotor speed. While the edgewise strain is higher for all cases, the difference between edge and flapwise strain decreases at higher wind speeds. This trend can be a result of blade pitch control that is imposed at high wind speeds.

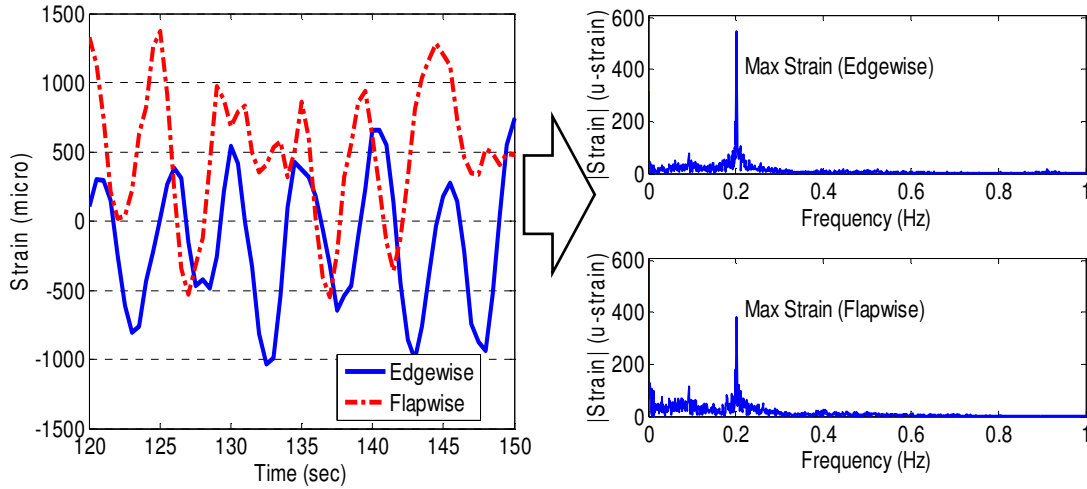


Figure 3. Strain vs. Time at 15.9 m from hub (Left) and Single sided amplitude spectrum in frequency of each flexing mode (Right): Data shown for NREL offshore turbine at 24 m/s wind speed and low turbulence.

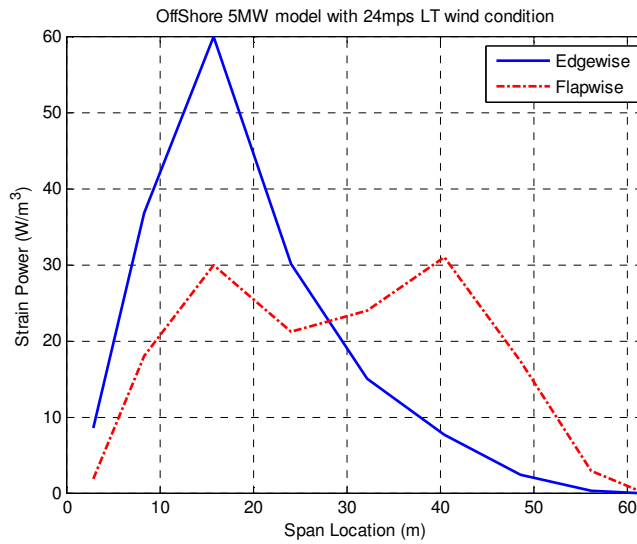


Figure 4. Edgewise and Flapwise strain power in an offshore blade as a function of blade location. Data are obtained during operational cycles corresponding to the maximum peak amplitude.

These results can be used to determine EH design requirements given the energy available and power transmission requirements. In **Figure 5**, the energy harvester design factor EH is shown as a function of the charging time Δt . Curves for three power levels P_{avail} , 13, 22 and 50 W/m³, are shown in the figure. These power levels are typical for the wind turbines investigated in the present work (see **Table 2**). In this case, a data transmission energy requirement of 280 μJ was selected, corresponding to the power required to transmit a single measurement via EH-link from Microstrain¹¹ (a commercially available wireless transmission module). The curves, then, are obtained by setting the transmission energy equal to the strain energy harvested W_{strain} (Eq. (4)). As an example, consider a ZnO

Table 2. Maximum Strain results for various turbines and wind conditions ($E_0 = 1$ GPa)

Load Condition	EDGE ($\mu\epsilon$)	FREQ (Hz)	$E_0^* \epsilon^{2*f}$ [W/m^3]	Max Span Loc. (m, %)	FLAP ($\mu\epsilon$)	FREQ (Hz)	$E_0^* \epsilon^{2*f}$ [W/m^3]	Max Span Loc. (m, %).
WT Model	CART3 (600 kW)							
6 m/s HT (High Turb)	90	0.27	2.19	7.5m (38%)	14	0.27	0.05	7.5m (38%)
6 m/s LT (Low Turb)	109	0.29	3.45	7.5m (38%)	17	0.29	0.08	7.5m (38%)
13 m/s HT	99	0.62	6.08	7.5m (38%)	38	0.62	0.90	7.5m (38%)
13 m/s LT	85	0.62	4.48	7.5m (38%)	32	0.62	0.63	7.5m (38%)
24 m/s HT	238	0.63	35.69	7.5m (38%)	218	0.63	29.94	7.5m (38%)
24 m/s LT	249	0.62	38.44	7.5m (38%)	220	0.62	30.01	7.5m (38%)
WT Model	WindPACT (1.5 MW)							
6 m/s HT	105	0.19	2.09	7.3m (21%)	20	0.21	0.08	11.7m (33%)
6 m/s LT	174	0.19	5.75	7.3m (21%)	20	0.19	0.08	11.7m (33%)
11.5 m/s HT	181	0.34	11.14	7.3m (21%)	56	0.34	1.07	16.2m (46%)
11.5 m/s LT	169	0.34	9.71	7.3m (21%)	37	0.34	0.47	11.7m (33%)
24 m/s HT	295	0.34	29.59	7.3m (21%)	156	0.34	8.27	16.2m (46%)
24 m/s LT	304	0.34	31.42	7.3m (21%)	168	0.34	9.60	16.2m (46%)
WT Model	NREL Offshore (5 MW)							
6 m/s HT	312	0.13	12.65	15.9m (25%)	55	0.13	0.39	15.9m (25%)
6 m/s LT	355	0.13	16.38	15.9m (25%)	59	0.13	0.45	15.9m (25%)
11.4 m/s HT	432	0.2	37.32	15.9m (25%)	178	0.2	6.34	40.5m (64%)
11.4 m/s LT	469	0.2	43.99	15.9m (25%)	163	0.2	5.31	15.9m (25%)
24 m/s HT	515	0.2	53.05	15.9m (25%)	352	0.2	24.78	40.5m (64%)
24 m/s LT	545	0.2	59.41	15.9m (25%)	393	0.2	30.89	40.5m (64%)

nanowire EH¹⁰ with an efficiency of 6.8%, volume of 0.38 mm³, and a modulus of 30 GPa, such that the design factor is 0.78 mm³. The corresponding charging time is approximately 2 hours for a harvester located on 5 MW offshore wind turbine operating at 24 m/s (providing approximately 50 W/m³ power). For wind turbine conditions or locations in which less power is available, the charging time requirements are approximately 4.5 hours for $P_{avail} = 20$ W/m³ and 7.5 hours for $P_{avail} = 13$ W/m³.

V. Conclusion

The present study provides an estimate of the strain energy that can be expected for typical wind turbine geometries over a range of wind loading conditions. Based on the FAST simulation results, the maximum strain occurs at a distance from the hub that is approximately 20 to 33% of the blade length. For the three turbine models, the maximum strain amplitude is 550 micro-strain at 0.34 Hz for the 5MW offshore turbine. On going work as part of the EOLOS²¹ facility at the University of Minnesota will include strain data from a fully instrumented 2.5 MW wind turbine. The estimates of strain energy from the current study along with the data from the full scale instrumented wind turbine will inform energy harvester design and development of data transmission algorithms.

Acknowledgments

This work was supported by the University of Minnesota Institute on the Environment, IREE Grant No. RS-0029-12 entitled “Development of self-powered wireless sensor for structural health monitoring in wind turbine blades.”

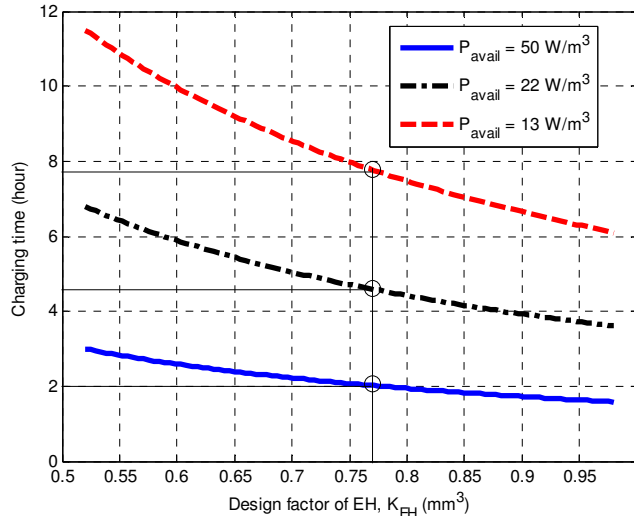


Figure 5. Energy Harvester Design Map for $W_{\text{strain}} = 280 \mu\text{J}$

References

- ¹Swisher, R., “Keys to Achieving 20 Percent Wind by 2030,” *Strategic Planning for Energy and the Environment* 28, 49, 2009.
- ²Ghoshal, A., Sundaresan, M. J., Schulz, M. J., Pai, P. F., “Structural health monitoring techniques for wind turbine blades,” *Journal of Wind Engineering and Industrial Aerodynamics* 85, 309, 2000.
- ³Khan, M. M., Iqbal, M. T., Khan, F., “Reliability and condition monitoring of a wind turbine,” *Instrumentation*, 1978, 2005.
- ⁴White, J., Adams, D., Rumsey, M., van Dam, J., Hughes, S., “Impact loading and damage detection in a carbon composite TX-100 wind turbine rotor blade,” *46th AIAA Aerospace Sciences Meeting and Exhibit*, Reno Nevada, 2008.
- ⁵Dutton, A., Blanch, M., Vionis, P., Lekou, D., Van Delft, D., Joosse, P., Anastassopoulos, A., Kouroussis, D., Kossivas, T., Philippidis, T., “Acoustic emission condition monitoring of wind turbine rotor blades: laboratory certification testing to large scale in-service deployment,” *European Wind Energy Conference*, 2003.
- ⁶Zayas, J. R., Paquette, J., Werlink, R. J., “Evaluation of NASA PZT Sensor/Actuator for Structural Health Monitoring of a Wind Turbine Blade,” *45th AIAA Aerospace Sciences Meeting*, Reno Nevada, 2007.
- ⁷Deines, K., Marinone, T., Schultz, R., Farinholt, K., Park, G., “Modal Analysis and SHM Investigation of CX-100 Wind Turbine Blade,” *Rotating Machinery, Structural Health Monitoring, Shock and Vibration* 5, 413, 2011.
- ⁸Rumsey, M. A., Paquette, J. A., “Structural health monitoring of wind turbine blades,” *Proceedings of SPIE* 6933, 2008.
- ⁹Ciang, C. C., Lee, J. R., Bang, H. J., “Structural health monitoring for a wind turbine system: a review of damage detection methods,” *Measurement Science & Technology* 19, 2008.
- ¹⁰Yang, R. S., Qin, Y., Dai, L. M., Wang, Z. L., “Power generation with laterally packaged piezoelectric fine wires,” *Nature Nanotechnology* 4, 34, 2009.
- ¹¹Microstrain, inc, <http://www.microstrain.com/energy-harvesting/eh-link> [cited 05 June 2012]
- ¹²Tadich, J. K., Wedel-Heinen, J., “Optimisation of blade testing – A practical application of damage tolerance,” *Proceedings of EWEC 2008: European Wind Energy Conference & Exhibition*, 2008.
- ¹³Poore, R., Lettenmaier, T., “Alternative Design Study Report: WindPACT Advanced Wind Turbine Drive Train Designs Study; November 1, 2000–February 28, 2002” National Renewable Energy Laboratory (NREL), Golden, CO., 2003.
- ¹⁴Schroeder, K., Ecke, W., Apitz, J., Lembke, E., Lenschow, G., “A fibre Bragg grating sensor system monitors operational load in a wind turbine rotor blade,” (Institute of Physics Publishing, 2006), vol. 17, pp. 1167-1172.
- ¹⁵Sandia National Laboratory, *NuMAD (Numerical Manufacturing And Design Tool)*. 2012.
- ¹⁶Jonkman, J. M., Buhl Jr, M. L., “FAST user’s guide,” *Rep. No. NREL/EL-500-38230, NREL, Golden, Colorado, USA*, 2005.
- ¹⁷NWTC Design Codes (AeroDyn by Dr. David J. Laino). <http://wind.nrel.gov/designcodes/simulators/aerodyn/>. Last modified 21 Feb 2012.

¹⁸Wright, A. D., Fingersh, L. J., “Advanced control design and field testing for wind turbines Part I: Control Design, Implementation, and Initial Tests” National Renewable Energy Laboratory, USA

¹⁹Malcolm, D. J., Hansen, A. C., “WindPACT Turbine Rotor Design Study,” June 2000–June 2002 (Revised). NREL/SR-500-32495. Golden, CO: NREL, 2006.

²⁰Jonkman, J., Butterfield, S., Musial, W., Scott, G., “Definition of a 5-MW reference wind turbine for offshore system development” National Renewable Energy Laboratory, USA, 2009.

²¹EOLOS Wind Energy Research Consortium, <http://www.eolos.umn.edu/> [cited 01 Nov 2012]